

Scattering cluster wave functions on the lattice using the adiabatic projection method

Alexander Rokash,^{1,*} Michelle Pine,^{2,†} Serdar Elhatisari,^{3,2,‡}
Dean Lee,^{2,§} Evgeny Epelbaum,^{1,¶} and Hermann Krebs^{1,**}

¹*Institut für Theoretische Physik II, Ruhr-Universität Bochum, 44870 Bochum, Germany*

²*Department of Physics, North Carolina State University, Raleigh, North Carolina 27695, USA*

³*Helmholtz-Institut für Strahlen- und Kernphysik
(Theorie) and Bethe Center for Theoretical Physics,
Universität Bonn, 53115 Bonn, Germany*

(Dated: July 26, 2018)

The adiabatic projection method is a general framework for studying scattering and reactions on the lattice. It provides a low-energy effective theory for clusters which becomes exact in the limit of large Euclidean projection time. Previous studies have used the adiabatic projection method to extract scattering phase shifts from finite periodic-box energy levels using Lüscher's method. In this paper we demonstrate that scattering observables can be computed directly from asymptotic cluster wave functions. For a variety of examples in one and three spatial dimensions, we extract elastic phase shifts from asymptotic cluster standing waves corresponding to spherical wall boundary conditions. We find that this approach of extracting scattering wave functions from the adiabatic Hamiltonian to be less sensitive to small stochastic and systematic errors as compared with using periodic-box energy levels.

PACS numbers: 21.60.De,04.60.Nc,25.55.-e

I. INTRODUCTION

Ab initio description of scattering and reactions involving nuclei is one of the major challenges in computational nuclear physics. Recent progress along this line has been achieved using resonating group methods [1–3], fermionic molecular dynamics [4, 5], the coupled-cluster expansion, see [6] for a review article, and variational and Green's function Monte Carlo methods [7, 8]. For calculations involving lattice methods, there has been progress in using finite periodic volumes to analyze coupled-channel scattering [9–15] and three-body

*Electronic address: alexander.rokash@ruhr-uni-bochum.de

†Electronic address: mjmantoo@ncsu.edu

‡Electronic address: selhati@ncsu.edu

§Electronic address: dean.lee@ncsu.edu

¶Electronic address: evgeny.epelbaum@ruhr-uni-bochum.de

**Electronic address: hermann.krebs@ruhr-uni-bochum.de

systems [16–18]. In this paper we concentrate on the adiabatic projection method for calculating nuclear reactions from lattice simulations in the framework of chiral effective field theory (EFT). See [19–22] for some recent results using lattice EFT. The general strategy in the adiabatic projection formalism as formulated in the pioneering work [23–25] involves two steps. First, one uses the Euclidean time projection method to determine an adiabatic Hamiltonian for the participating nuclei starting from the microscopic Hamiltonian derived in chiral EFT. In the second step, one uses a technique such as Lüscher’s finite-volume method [26, 27] to extract the corresponding scattering phase shifts [24].

The adiabatic projection formalism has been successfully benchmarked against continuum calculations for fermion-dimer scattering. However for heavier systems, Lüscher’s finite-volume energy approach for extracting scattering phase shifts is expected to suffer from potentially large errors due to stochastic and systematic uncertainties in the lattice Monte Carlo energies. In this paper, we explore various techniques to access scattering on the lattice that do not require a high-accuracy determination of the energy spectrum. For simple three-body systems in one and three dimensions, we demonstrate that scattering phase shifts can be reliably extracted from the asymptotic cluster wave functions within the adiabatic projection method.

Our paper is organized as follows. We begin with introducing the adiabatic projection method in some detail in section II. Section III describes Lüscher’s finite volume method, while section IV describes the extraction of the asymptotic cluster wave functions on the lattice. The microscopic Hamiltonian used in our work is specified in section V, which also provides details on the computation of the adiabatic Hamiltonian. Various approaches for extracting the two-cluster elastic scattering phase shifts in one and three spatial dimensions on the lattice are introduced and applied in sections VI and VII, respectively. Finally, the main results of our study are summarized in section VIII.

II. THE ADIABATIC PROJECTION METHOD

The adiabatic projection method treats the cluster-cluster scattering problem on the lattice by using Euclidean time projection to determine an adiabatic Hamiltonian for the participating clusters. When the temporal lattice spacing is nonzero, an adiabatic transfer matrix rather than the Hamiltonian is constructed, but the method is essentially the same. We start with an L^3 periodic lattice and set of two-cluster states $|\vec{R}\rangle$ labeled by their separation vector \vec{R} , as illustrated in Fig. 1. In general, there are spin and flavor indices for these states, but we suppress writing the indices for notational simplicity. The exact form of these two-cluster states is not important except that they are localized so that for large separations they factorize as a tensor product of two individual clusters,

$$|\vec{R}\rangle = \sum_{\vec{r}} |\vec{r} + \vec{R}\rangle_1 \otimes |\vec{r}\rangle_2. \quad (1)$$

These states are propagated in Euclidean time to form dressed cluster states,

$$|\vec{R}\rangle_\tau = \exp(-H\tau)|\vec{R}\rangle. \quad (2)$$

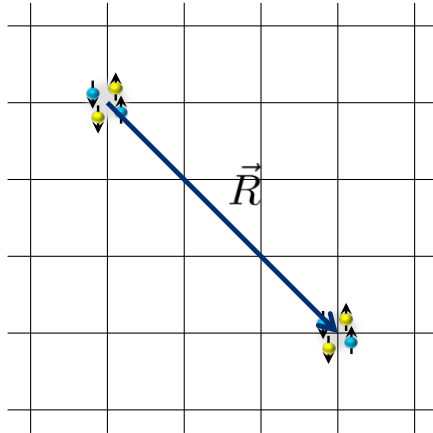


Figure 1: (Color online) Two-body cluster initial state $|\vec{R}\rangle$ separated by the displacement vector \vec{R} .

By evolving in Euclidean time with the microscopic Hamiltonian, deformations and polarizations of the interacting clusters are incorporated automatically, and we are projecting onto the space of low-energy scattering states in our finite volume. In the limit of large Euclidean time, these dressed cluster states span the low-energy subspace of two-cluster continuum states.

We evaluate matrix elements of the microscopic Hamiltonian with respect to the dressed cluster states,

$$[H_\tau]_{\vec{R},\vec{R}'} = {}_\tau\langle\vec{R}|H|\vec{R}'\rangle_\tau. \quad (3)$$

Since the dressed cluster states $|\vec{R}\rangle_\tau$ are, in general, not orthogonal, we construct a norm matrix N_τ given by the inner product

$$[N_\tau]_{\vec{R},\vec{R}'} = {}_\tau\langle\vec{R}|\vec{R}'\rangle_\tau. \quad (4)$$

From this a Hermitian adiabatic Hamiltonian matrix can be defined using the inverse square root of the norm matrix,

$$[H_\tau^a]_{\vec{R},\vec{R}'} = \sum_{\vec{R}'',\vec{R}'''} [N_\tau^{-1/2}]_{\vec{R},\vec{R}''} [H_\tau]_{\vec{R}'',\vec{R}'''} [N_\tau^{-1/2}]_{\vec{R}''',\vec{R}'}. \quad (5)$$

In the limit of large τ , the spectrum of H_τ^a exactly reproduces the low-energy finite volume spectrum of the microscopic Hamiltonian H . So for the elastic phase shifts, one can take the spectrum of H_τ^a and apply the finite-volume scaling analysis developed by Lüscher [26, 27].

III. LÜSCHER'S FINITE-VOLUME METHOD

The Lüscher method [26, 27] relates the two-body scattering states in periodic finite volume to the scattering parameters in the infinite volume and continuum limits. The main idea behind the derivation of this method is to use the known asymptotic form of the wave

function for a short range interaction and the periodicity of the system. The one-dimensional result of this ansatz is [26]

$$e^{2i\delta(p)} = e^{-ipL}, \quad (6)$$

where p is the relative momenta between two clusters¹, $\delta(p)$ is the scattering phase shift, and we assume the total momentum of the two-cluster system to be zero. In three dimensions, the situation is more complicated due to breaking of the rotational invariance by the cubic symmetry of finite periodic box. The scattering phase shifts are directly related to the momentum via the formula [26, 27]

$$p \cot \delta_\ell(p) = \frac{1}{\pi L} S(\eta) \quad \text{for } \ell = 0, 1, \quad (7)$$

where $\eta = \left(\frac{Lp}{2\pi}\right)^2$ and $S(\eta)$ is three-dimensional zeta function,

$$S(\eta) = \lim_{\Lambda \rightarrow \infty} \left[\sum_{\vec{n}} \frac{\theta(\Lambda^2 - \vec{n}^2)}{\vec{n}^2 - \eta} - 4\pi \Lambda \right], \quad (8)$$

or, in the exponentially accelerated form [26–28],

$$S(\eta) = 2\pi^{3/2} e^\eta (2\eta - 1) + e^\eta \sum_{\vec{n}} \frac{e^{-|\vec{n}|^2}}{|\vec{n}|^2 - \eta} - \pi^{3/2} \int_0^1 d\lambda \frac{e^{\lambda\eta}}{\lambda^{3/2}} \left(4\lambda^2 \eta^2 - \sum_{\vec{n}} e^{-\pi^2 |\vec{n}|^2 / \lambda} \right). \quad (9)$$

The relation between the relative momentum appearing in Eq. (7)–(9) and the finite-volume energies for $\ell = 0$ is given by [35, 36]

$$E(p, L) = \frac{p^2}{2\mu} - B_1 - B_2 + \bar{\tau}_1(\eta) \Delta E_1(L) + \bar{\tau}_2(\eta) \Delta E_2(L), \quad (10)$$

where μ is the reduced mass of the system, B_i is the binding energy of the cluster $i = \{1, 2\}$ in the infinite volume limit, $\Delta E_i(L) = E_i(L) + B_i$ is the finite volume energy shifts of the clusters in the rest frame, and $\bar{\tau}_i(\eta)$ is the topological correction factor to the energy of the cluster i ,

$$\bar{\tau}(\eta) = \frac{1}{\sum_{\vec{k}} (\vec{k}^2 - \eta)^{-2}} \sum_{\vec{k}} \frac{\sum_{i=1}^3 \cos(2\pi k_i \alpha)}{3(\vec{k}^2 - \eta)^2}. \quad (11)$$

In Ref. [25], it was found that for $\ell > 0$, the topological corrections are suppressed by the size of the finite volume, $\bar{\tau}(\eta) = 1 + \mathcal{O}(1/L)$, so that Eq. (10) becomes

$$E(p, L) = \frac{p^2}{2\mu} + E_1(L) + E_2(L). \quad (12)$$

¹ Clusters refer to either a point-like particle or a composite particle as a bound state of several particles.

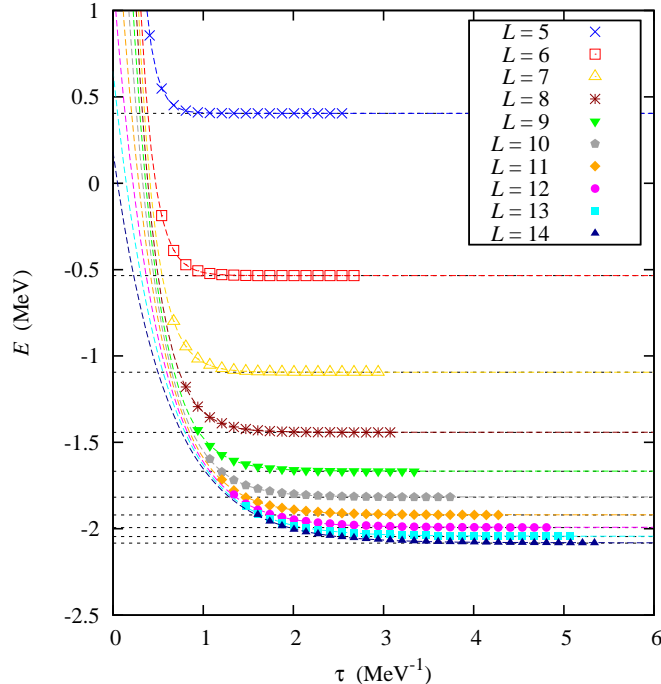


Figure 2: (Color online) The colored data points show the lowest energy levels of the adiabatic Hamiltonian versus projection time τ for the dimer-fermion system on various L^3 periodic lattices. The horizontal black-dashed lines are the lowest energy levels of the microscopic Hamiltonian for the same L^3 lattices. The dimer energy is -2.2246 MeV and the lattice spacing is 1.97 fm.

To minimize potential errors in the calculations using the Lüscher's method, we also take into account the effective mass of the clusters on the lattice. Lüscher's method is a useful and commonly used tool for calculating scattering parameters. For examples of recent extensions and generalizations of Lüscher's original work see Ref. [11–15, 28–31].

The simple elegance of Lüscher's method is that all of the information regarding scattering phase shifts is encoded into finite-volume energy values. This simplicity can, however, be a weakness when applied to scattering processes relevant to low-energy nuclear physics. The problem is that the binding energies of the scattering nuclei can be anywhere from a few MeV to tens or hundreds of MeV, while the finite-volume scattering energy shifts can be as small as a few keV. The problem is even more difficult in lattice QCD calculations where the rest energy of the nucleons is also part of the calculations.

Thus, while the scattering data is encoded in the finite-volume energy and waiting to be extracted, the finite-volume energy value is prone to several sources of potentially large errors. In Fig. 2, we show the lowest-lying energy state for a dimer-fermion system versus projection time τ for various L^3 periodic lattices. The dimer energy is set to be -2.2246 MeV and the lattice spacing is 1.97 fm. We consider this example in detail later in our discussion. The point we emphasize here is that in order to measure the s -wave scattering phase shift to an error of a few degrees, we need to measure the finite-volume energy to an accuracy of about 10 keV. In this simple three-particle calculation we are using exact matrix methods, and there are no stochastic errors. However, in a typical large-scale Monte Carlo calculation,

there are stochastic errors that grow exponentially with projection time τ . The stochastic errors are much reduced in a constrained Monte Carlo calculation using, for example, fixed fermionic nodal constraints. However here we have a different problem that the scattering energies may be artificially shifted by the constraints. In addition to these issues, there are also corrections to the binding energies of the scattering nuclei due to the finite volume [32–36].

In view of the problems with finite-volume energy calculations for low-energy nuclear scattering, we introduce in this paper another approach for extracting scattering phase shifts which directly analyzes cluster wave functions generated by the adiabatic Hamiltonian. This approach has the advantage of being far less sensitive to small errors in reproducing the binding energy and detailed structure of the participating nuclei.

IV. ASYMPTOTIC CLUSTER WAVE FUNCTIONS

For each particle of mass m , the microscopic Hamiltonian contains a kinetic energy term of the form $-\vec{\nabla}^2/(2m)$ or, more precisely, the lattice approximation to this operator. Therefore the Euclidean-time evolution operator $\exp(-H\tau)$ acts as a diffusion operator with diffusion constant inversely proportional to the particle mass m . Since the particles are diffusing in space as a function of Euclidean time, it is necessary to be precise about what we mean by widely-separated clusters at asymptotically large distances.

In order to explain the various time and length scales of our asymptotic wave function analysis, it is useful to first specify a relative error tolerance, ϵ , for all steps in our cluster-cluster scattering calculation. As we project to large Euclidean time, any isolated single-cluster initial state will simply relax into the ground state of that cluster system. We define τ_ϵ as the time at which the relative contamination due to excited cluster states is less than ϵ .

We now consider applying Euclidean time projection for the time duration τ_ϵ in order to remove excited cluster states. During the time interval τ_ϵ , each cluster undergoes spatial diffusion by an average distance proportional to $\sqrt{\tau_\epsilon/M}$, where M is the mass of the cluster. We call this distance the diffusion length. Let $d_{\epsilon,1}$ be the diffusion length for the first cluster, and $d_{\epsilon,2}$ be the diffusion length for the second cluster. In order to have some widely-separated clusters, we take our periodic box length L to be much larger than $d_{\epsilon,1}$ and $d_{\epsilon,2}$. We recall that \vec{R} is the initial separation vector between the two clusters. When $|\vec{R}| \gg d_{\epsilon,1}, d_{\epsilon,2}$ the dressed cluster state $|\vec{R}\rangle_{\tau_\epsilon}$ consists of non-overlapping clusters. We thus can define an asymptotic radius R_ϵ as the radius such that for $|\vec{R}| > R_\epsilon$ the amount of overlap between the cluster wave packets is less than ϵ .

In the asymptotic region $|\vec{R}| > R_\epsilon$, our dressed clusters are widely separated and interact only through long range forces such as the Coulomb interaction. Therefore, we can describe our system in terms of an effective cluster Hamiltonian H^{eff} that is simply a free lattice Hamiltonian for two point particles accompanied by the long-range interactions inherited

from the microscopic Hamiltonian. So in the asymptotic region we have

$$[N_\tau]_{\vec{R},\vec{R}'} = c \left[e^{-2H^{\text{eff}}\tau} \right]_{\vec{R},\vec{R}'}, \quad (13)$$

$$[H_\tau]_{\vec{R},\vec{R}'} = c \left[e^{-H^{\text{eff}}\tau} H^{\text{eff}} e^{-H^{\text{eff}}\tau} \right]_{\vec{R},\vec{R}'}, \quad (14)$$

where the coefficient c is given by the overlap of the initial single-cluster states in Eq. (1) with the exact single-cluster energy eigenstates. Since

$$[N_\tau^{-1/2}]_{\vec{R},\vec{R}'} = c^{-1/2} \left[e^{H^{\text{eff}}\tau} \right]_{\vec{R},\vec{R}'}, \quad (15)$$

we conclude that the adiabatic Hamiltonian coincides with the effective cluster Hamiltonian in the asymptotic region,

$$[H_\tau^a]_{\vec{R},\vec{R}'} = [H^{\text{eff}}]_{\vec{R},\vec{R}'}. \quad (16)$$

This last result is quite significant. We are using Euclidean time projection to calculate the matrices N_τ and H_τ . This Euclidean time projection entails a considerable amount of diffusion of the clusters. However, in the asymptotic region, we are in essence inverting the diffusion process when computing the adiabatic Hamiltonian and are left with an effective cluster Hamiltonian in a position space basis.

For cases where there are no long range interactions, the scattering states of the adiabatic Hamiltonian are given by a superposition of Bessel functions in the asymptotic region. For the case with Coulomb interactions, the scattering states of the adiabatic Hamiltonian in the asymptotic region correspond to a superposition of Coulomb wave functions. In the rest of this paper we extract cluster-cluster phase shifts for a variety of different examples in one and three spatial dimensions. We use spherical hard wall boundaries placed at some large wall radius R_{wall} in the asymptotic region and determine phase shifts by analyzing the asymptotic scattering wave functions. As we will show in the following discussion, this method is robust and accurate even in cases where the corresponding finite-volume energies produce large errors using Lüscher's method.

V. LATTICE FORMALISM

A. Microscopic Hamiltonian

Throughout this work, we consider several systems, all of which are comprised of three point particles. For some cases the particles are distinguishable and in some cases not. We specify the quantum statistics explicitly at a later stage. We consider the limit of where the range of the interaction is negligible compared to the scattering length. Then, in the low-energy limit, the interaction between particles can be represented by a delta-function.

Let b_s and b_s^\dagger be the annihilation and creation operators for each particle species s , and let $\rho_s(\vec{r})$ be corresponding density operator,

$$\rho_s(\vec{r}) = b_s^\dagger(\vec{r})b_s(\vec{r}). \quad (17)$$

The Hamiltonian in D spatial dimensions has the form $H = H_0 + V$ where

$$H_0 = - \sum_s \int d^D r b_s^\dagger(\vec{r}) \frac{\vec{\nabla}^2}{2m_s} b_s(\vec{r}), \quad (18)$$

$$V = \sum_{s < s'} C_{s,s'} \int d^D r : \rho_s(\vec{r}) \rho_{s'}(\vec{r}) :, \quad (19)$$

and the $::$ symbols indicate normal ordering. On the lattice, we can write the Hamiltonian as $H = H_0 + V$ where

$$H_0 = \sum_s \sum_{\hat{l}} \sum_{\vec{n}} \frac{1}{2m_s} b_s^\dagger(\vec{n}) \left[2b_s(\vec{n}) - b_s(\vec{n} + \hat{l}) - b_s(\vec{n} - \hat{l}) \right], \quad (20)$$

$$V = \sum_{s < s'} \sum_{\vec{n}} C_{s,s'} : \rho_s(\vec{n}) \rho_{s'}(\vec{n}) : . \quad (21)$$

Here \hat{l} denotes lattice unit vectors along all possible spatial axes.

For $D > 1$, a regularization of ultraviolet divergences due to the zero-range interaction is needed and provided by the nonzero lattice spacing. We denote the spatial lattice spacing as a . Throughout this paper, we will write all quantities in lattice units, which are physical units multiplied by the corresponding power of a in order to render the combination dimensionless.

In this paper we consider two examples, the first in one dimension and the second in three dimensions. We have organized our discussion to discuss both examples together, illustrating the methods and results for both examples, one after the other. For both cases the lattice spacing is taken to be 1.97 fm or 0.0100 MeV^{-1} . For the one-dimensional example, we consider three distinguishable particles with equal masses and calculate the scattering between a particle of species 3 with a dimer composed of particle types 1 and 2. For this case we tune the coupling $C_{1,2}$ to produce a bound state with energy -2.0000 MeV . The couplings $C_{1,3}$ and $C_{2,3}$ are both set equal to exactly one-tenth of the coupling $C_{1,2}$.

For the three-dimensional example, we consider two species of fermions which we label with spins, \uparrow and \downarrow . In this case we calculate scattering between a \uparrow particle and dimer composed of particles \uparrow and \downarrow . The fermion-dimer system corresponds to the neutron-deuteron scattering in the spin-quartet channel at leading order of pionless effective field theory. Therefore, we set the coupling constant $C_{\uparrow,\downarrow}$ to a value for which the dimer energy has the value of the physical deuteron energy of -2.2246 MeV .

B. Adiabatic Hamiltonian

We now discuss the implementation of the adiabatic projection method using a set of initial cluster states as introduced in Eq. (1). The two examples we consider are a particle-dimer system in one dimension and a fermion-dimer system in three dimensions. For the one-dimensional particle-dimer system, the particle-dimer cluster states are defined as

$$|\phi_{\vec{R}}\rangle = \sum_{\vec{n}} b_1^\dagger(\vec{n}) b_2^\dagger(\vec{n}) b_3^\dagger(\vec{n} + \vec{R}) |0\rangle . \quad (22)$$

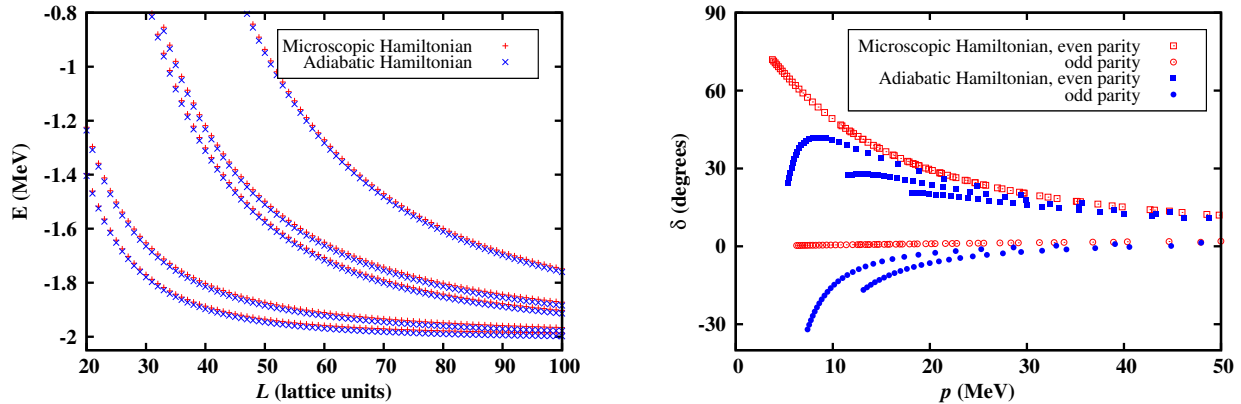


Figure 3: (Color online) Left panel: Finite-volume energies extracted from the microscopic Hamiltonian and the two-cluster adiabatic Hamiltonian for the particle-dimer system in one dimension. Right panel: The particle-dimer scattering phase shifts calculated from the data in the left panel using Lüscher’s method. Color online: Red (blue) symbols show the results corresponding to the original (adiabatic) Hamiltonian.

We use vector notation for notational consistency even though there is only one spatial direction. For the three-dimensional fermion-dimer system, we write the fermion-dimer initial cluster states as

$$|\phi_{\vec{R}}\rangle = \sum_{\vec{n}} b_{\uparrow}^{\dagger}(\vec{n}) b_{\downarrow}^{\dagger}(\vec{n}) b_{\uparrow}^{\dagger}(\vec{n} + \vec{R}) |0\rangle, \quad (23)$$

where $\vec{R} \neq 0$ because of Fermi statistics.

We now project the initial cluster states $|\phi_{\vec{R}}\rangle$ in Euclidean time τ using the microscopic Hamiltonian, H , for the respective systems. We use the Trotter approximation,

$$\exp(-H\tau) \approx (1 - a_t H)^{L\tau}, \quad (24)$$

where a_t is a time step parameter and $\tau = a_t L\tau$. For both the one-dimensional particle-dimer and three-dimensional fermion-dimer systems we have

$$|\phi_{\vec{R}}\rangle_{\tau} = (1 - a_t H)^{L\tau} |\phi_{\vec{R}}\rangle. \quad (25)$$

For large τ we obtain an accurate representation of the low-energy spectrum of H using the adiabatic Hamiltonian $[H_{\tau}^a]_{\vec{R}, \vec{R}'}$ defined in Eq. (5).

C. Scattering phase shifts from periodic-volume energy levels

In Fig. 3, we compare the energy spectrum of the microscopic Hamiltonian and the two-cluster adiabatic Hamiltonian for the particle-dimer system in one dimension for $\tau = 0.30 \text{ MeV}^{-1}$. We use the finite-volume energies to calculate the particle-dimer scattering phase shifts employing Lüscher’s method. Comparative results for the scattering phase

Table I: The lowest-lying energy and the corresponding scattering phase shifts for the dimer-fermion system computed using the Lüscher’s method for various periodic lattices. The energies E correspond to the microscopic Hamiltonian while the energies $E(\tau)$ correspond to the adiabatic Hamiltonian with projection time τ .

L	H		$[H_\tau^a]_{\vec{R}, \vec{R}'}$		
	E (MeV)	δ (degrees)	τ (MeV $^{-1}$)	$E(\tau)$ (MeV)	δ (degrees)
8	-1.4423319	-42.6	0.37	-1.4060289	-44.1
9	-1.6670941	-37.9	0.37	-1.6121233	-40.9
10	-1.8171997	-33.6	0.34	-1.7214154	-40.8
11	-1.9203247	-29.8	0.34	-1.8054714	-39.6
12	-1.9929256	-26.4	0.34	-1.8617182	-40.0

shifts are shown in the right panel of Fig. 3. Although the energy spectra of the adiabatic Hamiltonian and microscopic Hamiltonian are very similar, the resulting phase shifts have large differences at low energies. We also see a disagreement at low energies among phase shifts determined using different adiabatic Hamiltonian energy levels. This is because low-energy phase shifts are computed using very large box sizes L where the level spacing is small, and this magnifies any small discrepancies in the energy values.

We have performed a similar analysis for the fermion-dimer system in three dimensions. In Table I, we compare the lowest-lying energy states and resulting phase shifts computed using the microscopic Hamiltonian and adiabatic Hamiltonian for the dimer-fermion system. The energies E correspond to the microscopic Hamiltonian, while the energies $E(\tau)$ correspond to the adiabatic Hamiltonian. The scattering phase shifts are calculated using Lüscher’s method. As can be seen from Table I, the accuracy of the finite-volume energies is the range of 40–130 keV. However the relative error in the resulting phase shifts becomes as large as 50%.

Fortunately the adiabatic Hamiltonian contains more usable information than just periodic-lattice energy levels. As we show in Section VI, the scattering phase shifts can be determined with far better accuracy using the properties of the asymptotic scattering wave function.

VI. SCATTERING CLUSTER WAVE FUNCTION: METHODS

Borasoy *et al.* introduced a method to compute phase shifts for point-like particles on a lattice using a spherical wall boundary [37]. As done in the continuum [38], a spherical hard wall of radius R_{wall} is imposed on the relative separation of the two particles. In this study, we consider two-cluster systems, and the spherical hard wall boundary is imposed on the relative separation of the two clusters. For two clusters interacting via a potential of a finite-range R , the wave function at distances $r > R$ is given by

$$\Psi_\ell^{(p)}(r) = A_\ell \cos(pr + \delta_\ell - \ell\pi/2) \text{ for one dimension,} \quad (26)$$

$$\Psi_{\ell, m_\ell}^{(p)}(\vec{r}) = R_\ell^{(p)}(r) Y_{\ell, m_\ell}(\theta, \phi) \text{ for three dimensions,} \quad (27)$$

Table II: Irreducible representations of the cubic rotation group $\text{SO}(3, Z)$ and relation to spherical harmonics for $\ell \leq 2$.

$\text{SO}(3, Z)$	$\text{SO}(3)$	Y_{ℓ, m_ℓ}
A_1	$\ell = 0$	$\{Y_{0,0}\}$
T_1	$\ell = 1$	$\{Y_{1,-1}, Y_{1,0}, Y_{1,1}\}$
E_1	$\ell = 2$	$\{Y_{2,0}, (Y_{2,-2} + Y_{2,2})/\sqrt{2}\}$
T_2	$\ell = 2$	$\{Y_{2,1}, (Y_{2,-2} - Y_{2,2})/\sqrt{2}, Y_{2,-1}\}$

where p is the relative momentum of the clusters. For the one-dimensional case, there is no angular momentum, but we nevertheless use the notation $\ell = 0$ for even parity and $\ell = 1$ for odd parity. In three dimensions, the total wave function is decomposed into the radial part $R_\ell^{(p)}(r)$ and spherical harmonics $Y_{\ell, m_\ell}(\theta, \phi)$. The radial wave function $R_\ell^{(p)}(r)$ has the asymptotic form

$$R_\ell^{(p)}(r) = A_\ell [\cos \delta_\ell(p) j_\ell(pr) - \sin \delta_\ell(p) n_\ell(pr)] , \quad (28)$$

where A_ℓ is a normalization coefficient, and j_ℓ and n_ℓ denote spherical Bessel functions of the first and second kinds. Therefore, the three dimensional wave function in Eq. (27) can be rewritten as

$$\Psi_{\ell, m_\ell}^{(p)}(\vec{r}) = A_\ell Y_{\ell, m_\ell}(\theta, \phi) [\cos \delta_\ell(p) j_\ell(pr) - \sin \delta_\ell(p) n_\ell(pr)] . \quad (29)$$

In the asymptotic region, we fit Eq. (29) to the lattice wave functions emerging from imposing the spherical hard wall at radius R_{wall} . We evaluate the spherical harmonics $Y_{\ell, m_\ell}(\theta, \phi)$ on the lattice points, noting that there is no exact separation of radial and angular variables on the lattice. One must take into account the break up of the $2\ell + 1$ spin multiplets according to irreducible representations of the cubic rotation group [39, 40]. Irreducible representations of the $\text{SO}(3, Z)$ cubic rotation group are given in Table II for $\ell \leq 2$ [41].

For $\ell = 0$, the spherical harmonic $Y_{0,0}(\theta, \phi)$ is angle-independent, and we can directly match Eq. (29) to the lattice wave functions. However, for $\ell > 0$, the angular dependence makes the fitting more difficult. To resolve this issue, we use the identity

$$\sum_{m_\ell=-\ell}^{\ell} |Y_{\ell, m_\ell}(\theta, \phi)|^2 = \frac{2\ell + 1}{4\pi} . \quad (30)$$

Since the angular dependence drops out of this expression, it is convenient to work with the wave function probability distribution summed over m_ℓ ,

$$\sum_{m_\ell=-\ell}^{\ell} \left| \Psi_{\ell, m_\ell}^{(p)}(\vec{r}) \right|^2 = \frac{2\ell + 1}{4\pi} |A_\ell|^2 [\cos \delta_\ell(p) j_\ell(pr) - \sin \delta_\ell(p) n_\ell(pr)]^2 . \quad (31)$$

To obtain accurate results for the phase shifts within this approach, it is helpful to address some uncertainties in the precise location of the wall radius R_{wall} . While we impose a very

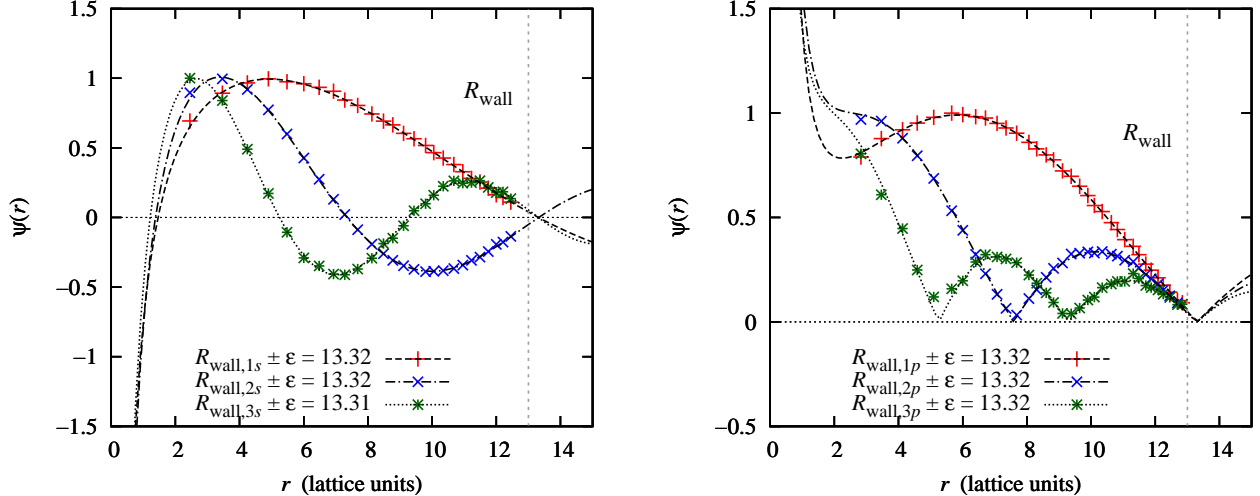


Figure 4: (Color online) First three lowest-lying s -state wave functions (left panel) and p -wave probability distributions (right panel) for the fermion-dimer system in three dimensions. A spherical hard wall is imposed at $R_{\text{wall}} = 13.0$ lattice units.

large but finite repulsive potential at distances $r \geq R_{\text{wall}}$, a close examination shows that wavefunction vanishes at some slightly larger radius $R'_{\text{wall}} = R_{\text{wall}} + \epsilon$, where ϵ is some fraction of a lattice spacing. This is illustrated in Fig. 4 for the lowest three s - and p -states of the fermion-dimer system in three dimensions. The hard wall potential is imposed for $r \geq R_{\text{wall}} = 13.0$ lattice units. We find that the first zero of the $1s$ wave function is at 13.32, the second zero of the $2s$ wave function is at 13.32, and the third zero of the $3s$ wave function is at 13.31 lattice units. For the first three lowest p -states, we find that corresponding zeros are all at 13.32 lattice units.

One can extract the scattering phase shifts by doing a three parameter fit of the overall normalization, momentum and phase shift to the interacting wave functions. We present the results of this fitting procedure later in our discussion. However, we have found more accurate results by making use of the empirical observation that R'_{wall} changes very little when going from the non-interacting system to the interacting system at approximately the same scattering energy. We first determine R'_{wall} from the lattice wave functions of the non-interacting cluster-cluster system. Then, using the same value of R'_{wall} , we fit the interacting wave functions using a two parameter fit to determine the phase shift of the interacting system using the relations

$$\delta_{\ell}(p) = \begin{cases} -pR'_{\text{wall}} + \frac{\pi(\ell+1)}{2} \pmod{\pi} & \text{for one dimension} \\ \tan^{-1} \left[\frac{j_{\ell}(pR'_{\text{wall}}/a)}{n_{\ell}(pR'_{\text{wall}}/a)} \right] & \text{for three dimensions.} \end{cases} \quad (32)$$

In Fig. 5, we show the $1s$ and $2s$ non-interacting particle-dimer wave functions used to calculate R'_{wall} and the corresponding interacting fermion-dimer wave functions used to determine the s -wave scattering phase shift $\delta_0(p)$.

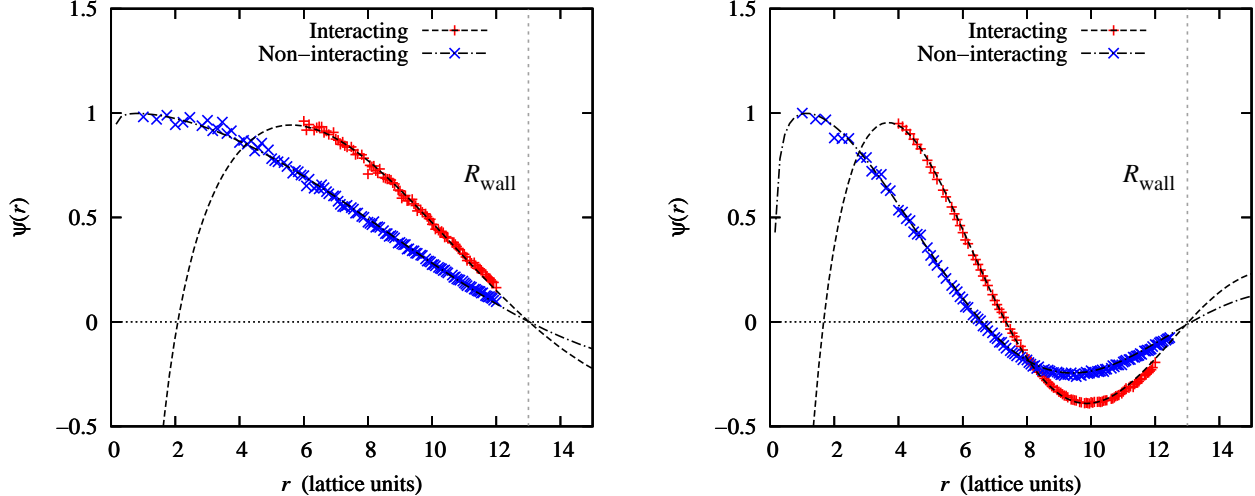


Figure 5: (Color online) Matching of the wave functions of the $1s$ - (left panel) and $2s$ -state (right panel). Free and interacting wave functions are denoted by (color online: blue) saltires and (color online: red) crosses, respectively.

VII. SCATTERING CLUSTER WAVE FUNCTION: PHASE SHIFT RESULTS

We now compute the scattering phase shifts using the adiabatic projection method and scattering cluster wave functions in our one-dimensional particle-dimer system and three-dimensional fermion-dimer system. The results are benchmarked against phase shifts extracted from the exact three-body energy spectrum obtained using Lüscher’s method. For the three-dimensional fermion-dimer system, the three-body energies are computed using the Lanczos iterative eigenvector method with a space of L^6 basis states. These can be viewed as exact lattice phase shifts. We note that while the adiabatic projection method calculations can be applied to much larger systems using lattice Monte Carlo, these exact Lanczos calculations are limited to small systems.

A. Particle-dimer scattering in one dimension

We make use of the simplicity of the one dimensional system to benchmark several different techniques for obtaining phase shifts. In each case we construct the adiabatic Hamiltonian using a projection time of $\tau = 0.30$ MeV. Lüscher’s energy spectrum method makes use of the energy of a scattering state and not its wave function. However we can also calculate phase shifts by fitting the wave function in the periodic box to its asymptotic form Eq. (26). Here and in what follows, we refer to this method as the Lüscher wave function method. In Fig. 6(a) we show an example of such a fit. The resulting value of the phase shift in this example is $\delta_0(p) = -160.5 \pm 0.3^\circ$ with momentum $p = 31.28 \pm 0.03$ MeV. We can compare the phase shifts obtained with this approach to Lüscher’s method using the exact energy spectrum. Fig. 6(b) shows Lüscher’s energy spectrum method phase shifts obtained for a number of lattices with $L = 6 \dots 100$ in lattice units. With the Lüscher periodic-

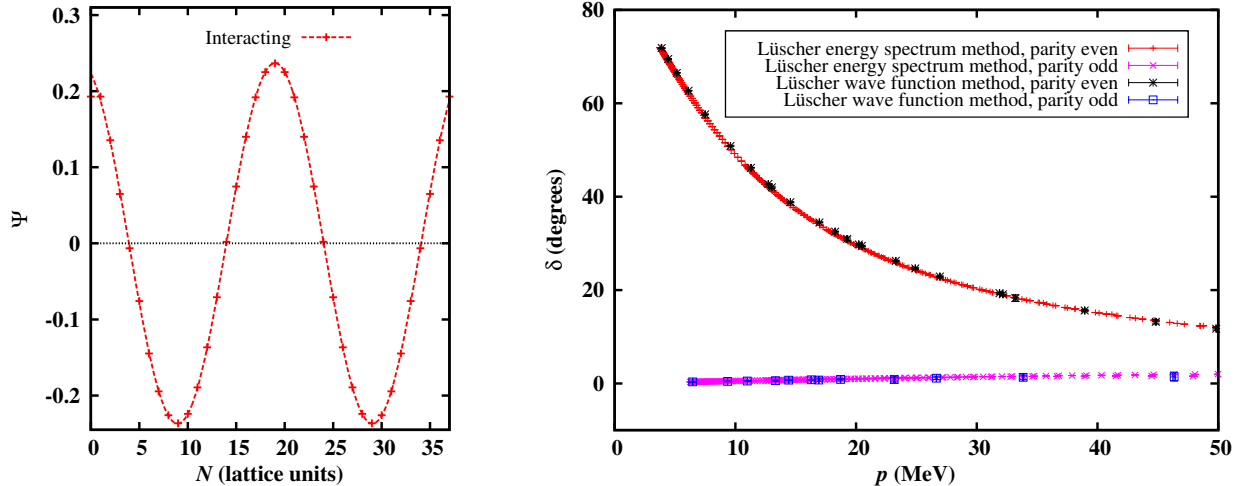


Figure 6: (Color online) Particle-dimer phase shifts in one dimension calculated using the Lüscher wave function method. Left panel: An example of the wave function matching. Right panel: Comparison of the phase shifts calculated using the Lüscher periodic-box wave function method and Lüscher’s finite-volume method with the exact energy spectrum.

box wave function method, phase shifts are calculated for $L = 10, 20, \dots, 100$ in lattice units. As expected, one observes very good agreement between the Lüscher energy spectrum method and the Lüscher wave function fit. While this method clearly works very well for the one-dimensional system, we find that fitting periodic-box wave functions is much more problematic and less accurate in three dimensions, especially for $\ell \geq 1$. This is most likely due to systematic errors arising from lattice spacing artifacts.

The second method we consider is the spherical wall approach described in the previous section. We impose a hard boundary on the relative separation and calculate the phase shifts from the properties of the standing wave functions. This method allows for the calculation of several data points per chosen lattice volume, since we can vary the value of the wall radius, R_{wall} . This represents an important computational advantage as compared to the Lüscher wave function method, especially for calculations in three dimensions. We will consider two versions of the spherical wall method. In the first version we do a three parameter fit of the overall normalization, momentum and phase shift of the interacting wave functions. Fig. 7 shows the application of this approach for the case $L = 50$ and $R_{\text{wall}} = 20$ in lattice units. The resulting value of the phase shift in this example is $\delta_0(p) = -163.0 \pm 0.4$ for the momentum $p = 36.17 \pm 0.07$ MeV. This method also shows very good agreement with Lüscher’s energy spectrum method. The phase shifts are calculated for $L = 50$ and $R_{\text{wall}} = 13 \dots 23$ in lattice units.

Our next approach is a second version of the spherical wall wave function method. In this case we determine $R'_{\text{wall}} = R_{\text{wall}} + \epsilon$ from the non-interacting particle-dimer wave function. In the example shown in Fig. 8, the boundary is set at $R_{\text{wall}} = 17$, and we find the wave function vanishes at $R'_{\text{wall}} = 17.901$, and the momentum of the free wave function is $p_0 = 43.874 \pm 0.02$ MeV. We then do a two-parameter fit to the interacting wave function and find $\delta_0(p) = -165.8 \pm 0.5$ for the momentum $p = 42.5 \pm 0.1$ MeV. The phase shifts shown in the right panel of Fig. 8 are calculated for $L = 50$ and $R_{\text{wall}} = 13 \dots 23$ in lattice units. The

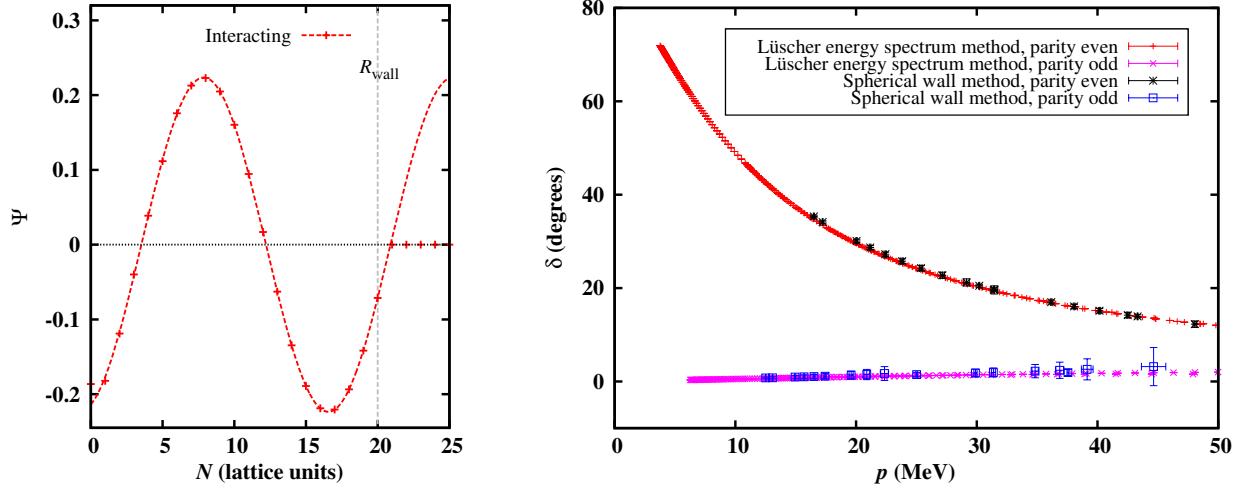


Figure 7: (Color online) Particle-dimer phase shifts in one dimension calculated using the spherical-wall method in one dimension with a three-parameter fit. Left panel: An example of the wave function fits. Right panel: Comparison of the phase shifts calculated using the spherical wall method and Lüscher’s finite-volume method with the exact energy spectrum.

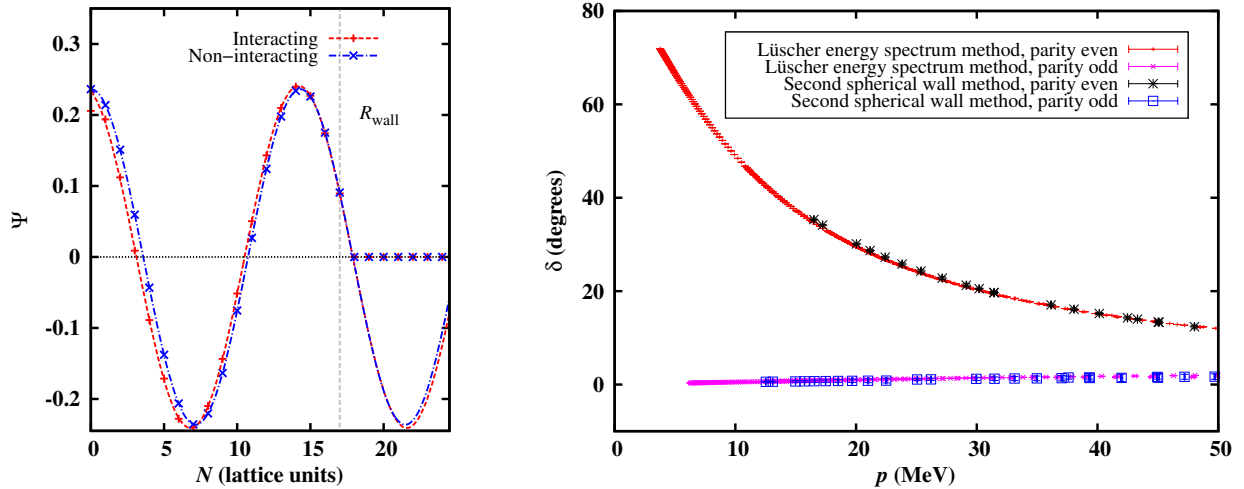


Figure 8: (Color online) Particle-dimer phase shifts in one dimension using the second spherical wall approach with R'_{wall} determined from the non-interacting wave function. Left panel: An example of the wave function fits. Right panel: Comparison of the phase shifts calculated using the second spherical wall approach and Lüscher’s finite-volume method with the exact energy spectrum.

results are in agreement with the results of the first spherical wall approach, but have smaller error bars, especially for the odd parity phase shifts. In three dimensions this improvement becomes more significant.

One of the disadvantages of the spherical wall method is that one needs to go to rather large values of R_{wall} and L in order to probe very low energies. The last method we consider overcomes this issue. In order to compute phase shifts at low momenta using small lattices, we impose a spherical hard wall and add also an attractive well potential in front of the

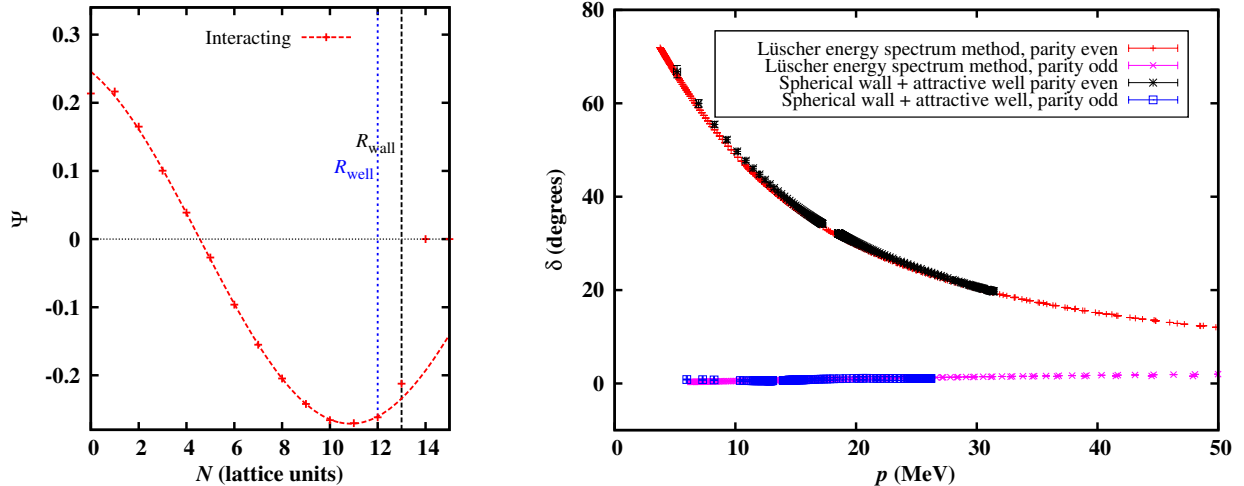


Figure 9: (Color online) Particle-dimer phase shifts in one dimension with the spherical wall and an attractive well potential. Left panel: An example of the wave function matching. Right panel: Comparison of the phase shifts calculated using the approach based on the combination of the spherical wall and attractive well with Lüscher’s finite-volume method using the exact energy spectrum.

wall boundary. We treat the depth of the well as an adjustable continuous parameter. The example shown in Fig. 9 corresponds to the case of $L = 30$, $R_{\text{wall}} = 13$ and $R_{\text{well}} = 12$ in lattice units. The resulting value of the phase shift in this example is $\delta_0(p) = -155.0 \pm 1.6^\circ$ at momentum $p = 24.9 \pm 0.6$ MeV. The phase shifts shown in the right panel of Fig. 9 are calculated for $L = 50$, $R_{\text{wall}} = 23$ and different well depths. The agreement with Lüscher’s energy spectrum method is very good, and we also obtain phase shifts for smaller momenta. However, the additional attractive potential distorts the asymptotic form of the wave function near the potential well. The distortion of the wave function grows with the depth of the attractive potential, and the calculation of the phase shifts for smaller momenta is achieved at the expense of a larger relative error. This might complicate the application of this method for calculations in three dimensions where the values of R_{wall} are typically smaller.

B. Fermion-dimer scattering in three dimensions

Before presenting lattice calculations for fermion-dimer scattering in three dimensions, we first review continuum calculations of the same system in the limit of zero range interactions. This corresponds to neutron-deuteron scattering at leading order in pionless effective field theory [42–44]. The T -matrix is obtained by solving the Skorniakov-Ter-Martirosian (STM)

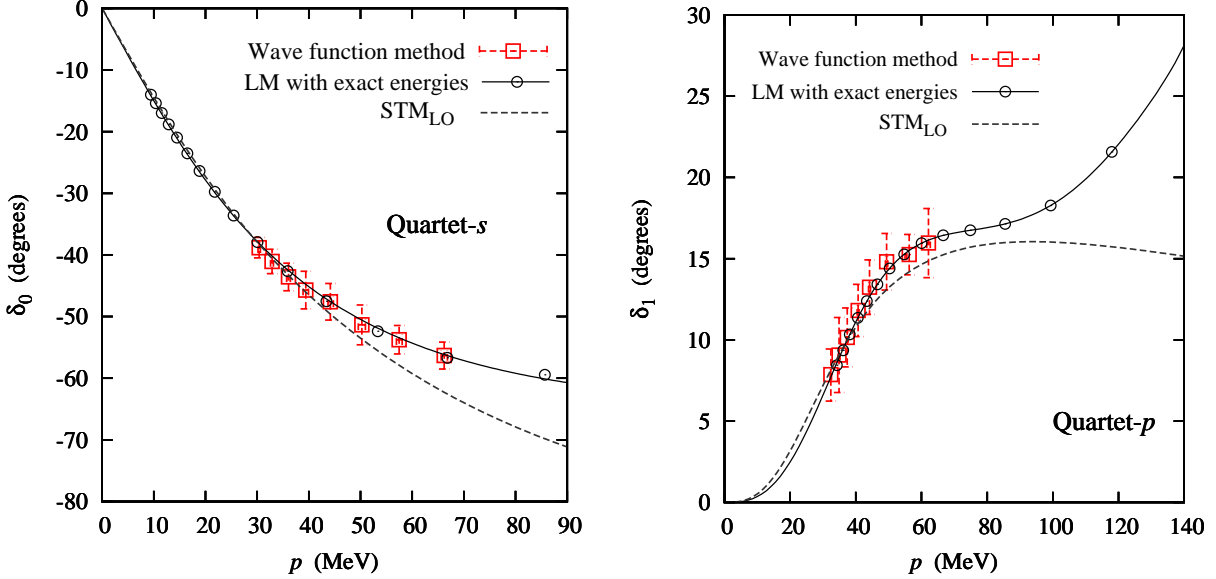


Figure 10: (Color online) The s -wave (left panel) and p -wave (right panel) scattering phase shifts for fermion-dimer scattering in three dimensions. We compare phase shifts calculated using the the spherical wall approach with R'_{wall} determined from the non-interacting wave function with Lüscher's finite-volume method using the exact energy spectrum.

integral equation,

$$T_\ell(k, p) = -\frac{8\pi\gamma}{mpk} Q_\ell \left(\frac{p^2 + k^2 - mE - i0^+}{pk} \right) - \frac{2}{\pi} \int_0^\infty dq \frac{q}{p} \frac{T_\ell(k, q)}{\sqrt{3q^2/4 - mE - i0^+} - \gamma} Q_\ell \left(\frac{p^2 + q^2 - mE - i0^+}{pq} \right), \quad (33)$$

where γ is the dimer binding momentum, $E = 3p^2/(4m) - \gamma^2/m$ is the total energy, and Q_ℓ is the Legendre function of the second kind,

$$Q_\ell(a) = \frac{1}{2} \int_{-1}^1 dx \frac{P_\ell(x)}{x+a}. \quad (34)$$

The scattering phase shift can then be extracted by matching the solution of Eq. (33) with the on-shell T -matrix

$$T_\ell(p, p) = \frac{3\pi}{m} \frac{p^{2\ell}}{p^{2\ell+1} \cot \delta_\ell - ip^{2\ell+1}}. \quad (35)$$

For the three-dimensional fermion-dimer calculation, we use only the most promising of the four approaches explored previously for the one dimensional system. This is the spherical wall method with R'_{wall} determined from the non-interacting wave function. In Fig. 10, the squares show lattice results for the s -wave and p -wave scattering phase shifts using adiabatic projection method with $\tau = 0.37$ and spherical wall method. The circles are the exact lattice results obtained using Lüscher's method applied to the energies of the microscopic

Hamiltonian H evaluated using Lanczos eigenvector iteration. The dashed lines correspond to leading order pionless EFT continuum results obtained using the STM equation. The solid lines are fits of the lattice data using an effective range expansion,

$$p^{2\ell+1} \cot \delta_\ell(p) = -\frac{1}{a_\ell} + \frac{1}{2} r_\ell p^2 + \mathcal{O}(p^4). \quad (36)$$

We note again that these exact Lanczos benchmark calculations using the energies of H are only possible in small systems. The adiabatic projection method is needed to probe much larger systems via lattice Monte Carlo. We have seen in Table I that when we use Lüscher's method to extract phase shifts from the adiabatic Hamiltonian energies, the errors are as large as 50% at low energies. In comparison with this, we observe much smaller error bars and excellent agreement between the adiabatic Hamiltonian results and the exact lattice phase shifts in Fig. 10. We should mention that the discrepancies between the lattice and continuum results at large momenta are nothing more than lattice spacing artifacts and would go away in the limit of vanishing lattice spacing.

VIII. SUMMARY AND CONCLUSIONS

In this paper we have presented a new method for computing scattering parameters directly from cluster wave functions. It allows us to bypass computation of the energy spectrum and thus to avoid potentially large errors in calculating low-energy nuclear scattering and reactions using the adiabatic projection method. We showed that the adiabatic Hamiltonian in the asymptotic region reduces to a simple cluster Hamiltonian in a position space basis. In this way we can extract scattering phase shifts directly from the scattering cluster wave functions.

We considered particle-dimer scattering in one dimension and fermion-dimer scattering in three dimensions. In the one dimensional particle-dimer example, we explored various versions of the adiabatic projection method using the cluster wave functions rather than the finite volume energies to extract phase shifts. First, we presented a simple matching of the adiabatic lattice wave function in periodic box to the asymptotic form in Eq. (26). We were able to accurately fit the wave function in the asymptotic region, and the calculated phase shifts were in good agreement with exact lattice phase shifts computed using Lüscher's energy method and the spectrum of the microscopic Hamiltonian. Next, we imposed a spherical hard wall boundary on the relative separation and matched the resulting wave function to Eq. (26). This approach was also found to agree accurately with the exact lattice phase shifts. We considered two variants of this spherical wall approach and found more accurate results when we use non-interacting cluster wave functions to determine R'_{wall} , the radius where the wave function vanishes. We also tried adding an attractive potential well in addition to the spherical hard wall boundary in order to be able to continuously vary the scattering energy. However, we found that this potential well distorts the wave function in the asymptotic region and results in larger errors of the phase shifts.

We then considered the dimer-fermion system in three spatial dimensions, which also corresponds to neutron-deuteron scattering in the spin-quartet channel. For this calculation we use adiabatic projection and the spherical wall method with R'_{wall} determined from the non-

interacting wave function. We find that this method gives good results for the phase shifts which agree well with the exact lattice phase shifts determined from Lanczos calculations of the spectrum of the microscopic Hamiltonian H .

In this paper we have shown that very-high-precision energy calculations are not needed for determining phase shifts, and one can instead use spherical wall boundaries to measure phase shifts directly from scattering cluster wave functions. The methods we have presented here are specially designed to be immediately useful for large-scale calculations of cluster-cluster scattering using lattice Monte Carlo. Since the writing of the original draft of this work, the methods described here have been combined with lattice Monte Carlo simulations to produce the first *ab initio* calculation of alpha-alpha scattering [45]. The adiabatic projection method is used to reduce an eight-body system of nucleons to a system of two alpha particles. There has also been significant improvements on the extraction of lattice phase shifts using the spherical wall method with auxiliary potentials such as attractive wells and complex-valued potentials for particles with spin and partial-wave mixing [46].

We are confident that more applications are possible which combine the adiabatic projection method and Monte Carlo methods for scattering and reactions over a diverse range of few- and many-body systems. We note, for example, recent developments using impurity lattice Monte Carlo [25, 47], which opens the possibility of *ab initio* calculations of impurity quasiparticle scattering in quantum many-body systems.

Acknowledgments

The authors thank U.-G. Meißner for valuable comments on the manuscript. This work was supported in part by the U.S. Department of Energy grant DE-FG02-03ER41260 (D.L. and M.P.), U.S. Department of Education GAANN Fellowship (M.P.), the Seventh Framework Programme of EU, the ERC project 259218 NUCLEAREFT (E.E. and A.R.) and the European Community-Research Infrastructure Integrating Activity “Study of Strongly Interacting Matter” (acronym HadronPhysics3, Grant Agreement n. 283286).

-
- [1] P. Navratil, R. Roth and S. Quaglioni, Phys. Rev. C **82**, 034609 (2010) [arXiv:1007.0525 [nucl-th]].
 - [2] P. Navratil and S. Quaglioni, Phys. Rev. Lett. **108**, 042503 (2012) [arXiv:1110.0460 [nucl-th]].
 - [3] C. Romero-Redondo, S. Quaglioni, P. Navratil and G. Hupin, Phys. Rev. Lett. **113**, 032503 (2014) [arXiv:1404.1960 [nucl-th]].
 - [4] T. Neff, Phys. Rev. Lett. **106**, 042502 (2011) [arXiv:1011.2869 [nucl-th]].
 - [5] T. Neff, H. Feldmeier and K. Langanke, Prog. Part. Nucl. Phys. **66**, 341 (2011) [arXiv:1011.2341 [nucl-th]].
 - [6] G. Hagen, T. Papenbrock, M. Hjorth-Jensen and D. J. Dean, Rept. Prog. Phys. **77**, no. 9, 096302 (2014) [arXiv:1312.7872 [nucl-th]].
 - [7] K. M. Nollett and R. B. Wiringa, Phys. Rev. C **83**, 041001 (2011) [arXiv:1102.1787 [nucl-th]].

- [8] J. Carlson, S. Gandolfi, F. Pederiva, S. C. Pieper, R. Schiavilla, K. E. Schmidt and R. B. Wiringa, arXiv:1412.3081 [nucl-th].
- [9] C. Liu, X. Feng and S. He, Int. J. Mod. Phys. A **21**, 847 (2006) [hep-lat/0508022].
- [10] M. Lage, U.-G. Meißner and A. Rusetsky, Phys. Lett. B **681**, 439 (2009) [arXiv:0905.0069 [hep-lat]].
- [11] R. A. Briceno, Z. Davoudi and T. C. Luu, Phys. Rev. D **88**, no. 3, 034502 (2013) [arXiv:1305.4903 [hep-lat]].
- [12] R. A. Briceno and Z. Davoudi, Phys. Rev. D **88**, no. 9, 094507 (2013) [arXiv:1204.1110 [hep-lat]].
- [13] R. A. Briceno, Z. Davoudi, T. C. Luu and M. J. Savage, Phys. Rev. D **88**, no. 11, 114507 (2013) [arXiv:1309.3556 [hep-lat]].
- [14] R. A. Briceno, Phys. Rev. D **89**, no. 7, 074507 (2014) [arXiv:1401.3312 [hep-lat]].
- [15] M. Döring, U.-G. Meißner, E. Oset and A. Rusetsky, Eur. Phys. J. A **48**, 114 (2012) [arXiv:1205.4838 [hep-lat]].
- [16] K. Polejaeva and A. Rusetsky, Eur. Phys. J. A **48**, 67 (2012) [arXiv:1203.1241 [hep-lat]].
- [17] R. A. Briceno and Z. Davoudi, Phys. Rev. D **87**, no. 9, 094507 (2013) [arXiv:1212.3398 [hep-lat]].
- [18] U.-G. Meißner, G. Rios and A. Rusetsky, Phys. Rev. Lett. **114**, no. 9, 091602 (2015) [arXiv:1412.4969 [hep-lat]].
- [19] E. Epelbaum, H. Krebs, D. Lee and U.-G. Meißner, Phys. Rev. Lett. **106**, 192501 (2011) [arXiv:1101.2547 [nucl-th]].
- [20] E. Epelbaum, H. Krebs, T. A. Lähde, D. Lee and U.-G. Meißner, Phys. Rev. Lett. **109**, 252501 (2012) [arXiv:1208.1328 [nucl-th]].
- [21] T. A. Lähde, E. Epelbaum, H. Krebs, D. Lee, U.-G. Meißner and G. Rupak, Phys. Lett. B **732**, 110 (2014) [arXiv:1311.0477 [nucl-th]].
- [22] E. Epelbaum, H. Krebs, T. A. Lähde, D. Lee, U.-G. Meißner and G. Rupak, Phys. Rev. Lett. **112**, no. 10, 102501 (2014) [arXiv:1312.7703 [nucl-th]].
- [23] G. Rupak and D. Lee, Phys. Rev. Lett. **111**, no. 3, 032502 (2013) [arXiv:1302.4158 [nucl-th]].
- [24] M. Pine, D. Lee and G. Rupak, Eur. Phys. J. A **49**, 151 (2013) [arXiv:1309.2616 [nucl-th]].
- [25] S. Elhatisari and D. Lee, Phys. Rev. C **90**, no. 6, 064001 (2014) [arXiv:1407.2784 [nucl-th]].
- [26] M. Lüscher, Commun. Math. Phys. **105**, 153 (1986).
- [27] M. Lüscher, Nucl. Phys. B **354**, 531 (1991).
- [28] T. Luu and M. J. Savage, Phys. Rev. D **83**, 114508 (2011) [arXiv:1101.3347 [hep-lat]].
- [29] Z. Fu, Phys. Rev. D **85**, 014506 (2012) [arXiv:1110.0319 [hep-lat]].
- [30] L. Leskovec and S. Prelovsek, Phys. Rev. D **85**, 114507 (2012) [arXiv:1202.2145 [hep-lat]].
- [31] M. Göckeler, R. Horsley, M. Lage, U.-G. Meißner, P. E. L. Rakow, A. Rusetsky, G. Schierholz and J. M. Zanotti, Phys. Rev. D **86**, 094513 (2012) [arXiv:1206.4141 [hep-lat]].
- [32] M. Lüscher, Commun. Math. Phys. **104**, 177 (1986).
- [33] S. König, D. Lee and H.-W. Hammer, Phys. Rev. Lett. **107**, 112001 (2011) [arXiv:1103.4468 [hep-lat]].
- [34] S. König, D. Lee and H.-W. Hammer, Annals Phys. **327**, 1450 (2012) [arXiv:1109.4577 [hep-lat]].
- [35] S. Bour, S. König, D. Lee, H.-W. Hammer and U.-G. Meißner, Phys. Rev. D **84**, 091503 (2011) [arXiv:1107.1272 [nucl-th]].
- [36] S. Bour, H.-W. Hammer, D. Lee and U.-G. Meißner, Phys. Rev. C **86**, 034003 (2012) [arXiv:1206.1765 [nucl-th]].

- [37] B. Borasoy, E. Epelbaum, H. Krebs, D. Lee and U.-G. Meißner, *Eur. Phys. J. A* **34**, 185 (2007) [arXiv:0708.1780 [nucl-th]].
- [38] J. Carlson, V. R. Pandharipande and R. B. Wiringa, *Nucl. Phys. A* **424**, 47 (1984).
- [39] B. N. Lu, T. A. Lähde, D. Lee and U.-G. Meißner, arXiv:1504.01685 [nucl-th].
- [40] B. N. Lu, T. A. Lähde, D. Lee and U.-G. Meißner, *Phys. Rev. D* **90**, no. 3, 034507 (2014) [arXiv:1403.8056 [nucl-th]].
- [41] R. C. Johnson, *Phys. Lett. B* **114**, 147 (1982).
- [42] P. F. Bedaque and H. W. Griesshammer, *Nucl. Phys. A* **671**, 357 (2000) [nucl-th/9907077].
- [43] F. Gabbiani, P. F. Bedaque and H. W. Griesshammer, *Nucl. Phys. A* **675**, 601 (2000) [nucl-th/9911034].
- [44] G. Rupak and X. W. Kong, *Nucl. Phys. A* **717**, 73 (2003) [nucl-th/0108059].
- [45] S. Elhatisari, D. Lee, G. Rupak, E. Epelbaum, H. Krebs, T. A. Lähde, T. Luu and U.-G. Meißner, arXiv:1506.03513 [nucl-th].
- [46] B. N. Lu, T. A. Lähde, D. Lee and U.-G. Meißner, arXiv:1506.05652 [nucl-th].
- [47] S. Bour, D. Lee, H.-W. Hammer and U.-G. Meißner, arXiv:1412.8175 [cond-mat.quant-gas].